A robust empirical model to estimate earthquake-induced excess pore water pressure in saturated and non-saturated soils

Lucia Mele, Anna Chiaradonna, Stefania Lirer & Alessandro Flora

Bulletin of Earthquake Engineering
Official Publication of the European Association for Earthquake Engineering

ISSN 1570-761X

Bull Earthquake Eng
DOI 10.1007/s10518-020-00970-5

Springer

Bulletin of Earthquake Engineering
https://doi.org/10.1007/s10518-020-00970-5

S.I.: THE H2020 EUROPEAN PROJECT LIQUEFACT

A robust empirical model to estimate earthquake-induced excess pore water pressure in saturated and non-saturated soils

Lucia Mele[1] · Anna Chiaradonna[2] · Stefania Lirer[3] · Alessandro Flora[1]

Received: 22 July 2020 / Accepted: 28 September 2020

Abstract
In engineering practice, the liquefaction potential of a sandy soil is usually evaluated with a semi-empirical, stress-based approach computing a factor of safety in free field conditions, defined as the ratio between the liquefaction resistance (capacity) and the seismic demand. By so doing, an estimate of liquefaction potential is obtained, but nothing is known on the pore pressure increments (often expressed in the form of normalized pore pressure ratio r_u) generated by the seismic action when the safety factor is higher than 1. Even though r_u can be estimated using complex numerical analyses, it would be extremely useful to have a simplified procedure to estimate them consistent with the stress-based approach adopted to check the safety conditions. This paper proposes such a procedure with reference to both saturated and unsaturated soils, considering the latter as soils for which partial saturation has been artificially generated with some ground improvement technology to increase cyclic strength and thus tackle liquefaction risk. A simple relationship between the liquefaction free field safety factor FS, and $r_u(S_r)$ is introduced, that generalizes a previous expression proposed by Chiaradonna and Flora (Geotech Lett, 2020. https://doi.org/10.1680/jgele.19.00032) for saturated soils. The new procedure has been successfully verified against some experimental data, coming from laboratory constant amplitude cyclic tests and from centrifuge tests with irregular acceleration time histories for soils having different gradings and densities.

Keywords Liquefaction · Excess pore pressure generation · Factor safety · Non-saturated soils

1 Introduction

Earthquake induced liquefaction is a phenomenon strongly linked to pore water pressure build-up within cohesionless soil layers during the seismic action. The simultaneous generation, dissipation, and redistribution of excess pore pressures within the layers of a soil deposit can significantly modify the seismic response of the whole deposit.

✉ Lucia Mele
lucia.mele@unina.it

Extended author information available on the last page of the article

Published online: 06 October 2020

Several relationships have been proposed in literature to predict the pore pressure build-up induced by cyclic loadings, traditionally divided in three groups: stress-based (Lee and Albaisa 1974; Seed et al. 1975b; Booker et al. 1976; Chameau and Clough 1983; Wang and Kavazanjian 1989; Liyanapathirana and Poulos 2002; Polito et al. 2008; Cetin and Bilge 2012), strain-based (Martin et al. 1975; Dobry et al. 1985) and energy-based models (Green et al. 2000; Baziar et al. 2011).

The first to be developed were the stress-based models that were calibrated on the results of cyclic stress-controlled tests (triaxial or simple shear tests). Such models link the excess pore pressure ratio, r_u (defined as the ratio between the pore pressure increment Δu and the initial effective overburden stress, σ'_{v0}) to the cycle ratio N/N_{liq}, where N is the number of loading cycles and N_{liq} is the number of cycles required to attain liquefaction. Generally, in the simplest models (De Alba et al. 1975; Seed et al. 1975a, b; Booker et al. 1976) only one parameter has to be calibrated on cyclic stress-controlled tests results. As an example, the expression of Booker has been reported below:

$$r_u = \frac{2}{\pi} \cdot arcsin\left(\frac{N}{N_{liq}}\right)^{\frac{1}{2\beta}} \tag{1}$$

where β is an empirical constant which depends on the soil type and test conditions and influences the shape of the curve r_u—$N/N_{liq.}$ This parameter can be calibrated from cyclic triaxial tests, although the authors recommended using a β equal to 0.7, especially for clean sands. However, several relationships have been introduced to take into account fines content (FC) and relative density (Dr) (Polito et al. 2008).

Based on the experimental observations of Youd (1972), who demonstrated that the densification of dry sands is ruled by cyclic strains rather than cyclic stress, strain-based methods have been developed. According to them, the generation of pore water pressure is controlled by the amplitude of cyclic shear strains and number of loading cycles.

Although stress and strain-based methods are simple forms, both suffer from the difficulty and uncertainty of converting the seismic motion in an equivalent number of uniform cycles.

This drawback can be overcome by energy-based methods (Green et al. 2000) in which r_u is related to the energy dissipated per unit volume of soil. However, such models are not simple to be calibrated on the basis of laboratory test results. In addition, some empirical correlations have been developed based on the energy released during a seismic event (Davis and Berrill 1982; Law et al. 1990).

Recently, an interesting and practical pore pressure model has been proposed by Chiaradonna and Flora (2020) to compute the pore pressure ratio in saturated sandy soils when the safety factor in free field conditions FS (defined as the ratio between the seismic load required to trigger liquefaction and the one expected from the earthquake) is larger than 1:

$$r_u = \frac{1.8}{\pi} arcsin\left(FS^{-\frac{1}{2b\beta}}\right) \quad with \quad FS \geq 1 \tag{2}$$

According to Eq. (2), the excess pore pressure ratio can be computed known FS, b and β, where the parameter b of Eq. (2) rules the slope of the cyclic resistance curve in the CRR:N_{liq} plane (Boulanger and Idriss 2014) and β is the parameter of the expression proposed by Booker et al. (1976) (Eq. 1) calculated according to Polito et al. (2008). The value of r_u corresponding to liquefaction triggering (FS = 1) will be named $r_{u,liq}$.

It is worth noting that in Eq. (2), the value 1.8 is used instead of the value 2 proposed by Booker et al. (1976) (Eq. 1) to accommodate the liquefaction triggering condition $r_{u,liq}=0.9$ herein assumed (while in the original work by Booker and coauthors liquefaction was assumed to happen at $r_{u,liq}=1$).

The safety factor FS is usually quantified by means of well-known stress-based semi-empirical correlations (Seed and Idriss 1971; Robertson and Wride 1998; Boulanger and Idriss 2014), in which both soil capacity and seismic demand are written as cyclic stress ratios (respectively CRR and CSR):

$$FS = \frac{CRR}{CSR} = \frac{CRR_{M=7,5,\sigma'v=1}}{CSR} \cdot MSF \cdot K_{\sigma} \cdot K_{\alpha} \tag{3}$$

where $CRR_{M=7.5,\sigma'v=1}$ is the soil capacity referred to a magnitude $M=7.5$ and to $\sigma'_v=103$ kPa, MSF is the magnitude scaling factor, introduced to account for the effect of the duration of the seismic event, K_σ and K_α are correcting factors to account respectively for the effective overburden stress and for an initial static shear stress on the horizontal plane. The expressions of all the factors of Eq. (3) are not reported here for the sake of brevity, and can be easily found in literature (e.g., NASEM 2016).

A comprehensive review of CPT-based and SPT-based liquefaction triggering procedures is reported by Boulanger and Idriss (2014), who proposed charts to quantify the cyclic resistance ratio $CRR_{M=7.5,\sigma'v=1}$ as:

$$CRR_{M=7.5,\sigma'_v=1} = \exp\left(\frac{q_{c1Ncs}}{113} + \left(\frac{q_{c1Ncs}}{1000}\right)^2 - \left(\frac{q_{c1Ncs}}{140}\right)^3 + \left(\frac{q_{c1Ncs}}{137}\right)^4 - 2.8\right) \tag{4a}$$

$$CRR_{M=7.5,\sigma'_v=1} = \exp\left(\frac{(N_1)_{60cs}}{14.1} + \left(\frac{(N_1)_{60cs}}{126}\right)^2 - \left(\frac{(N_1)_{60cs}}{23.6}\right)^3 + \left(\frac{(N_1)_{60cs}}{25.4}\right)^4 - 2.8\right) \tag{4b}$$

where q_{c1Ncs} and $(N_1)_{60cs}$ are respectively the corrected CPT tip resistance and the corrected SPT blow count counting for fine content effects (Idriss and Boulanger 2008; Boulanger and Idriss 2014). In the simplified procedure, CSR is expressed as:

$$CSR = 0.65\frac{a_{max}}{g}\frac{\sigma_v}{\sigma'_v}r_d \tag{5}$$

where σ_v and σ'_v are the vertical total and effective stresses at a depth z, a_{max} is the maximum horizontal acceleration, g is the gravity acceleration and r_d is a reduction factor accounting for soil deformability, whose expression can be found in Boulanger and Idriss (2014).

Since the expression of CRR has been empirically defined to bound experimental evidences of liquefaction, it often leads to a conservative estimate of the local safety conditions. Furthermore, it does not take into account the hydraulic interaction among contiguous layers during the seismic action: because of seismically induced pore pressures build up and of the subsequent unbalanced values of water head, a filtration mechanism may in fact add, with an overall modification of the pore pressure increments and therefore of the safety conditions (Cubrinovski et al. 2018). These drawbacks of the stress-based approach are nowadays well known, and alternative procedures to evaluate FS have been proposed in literature, mostly following an energy based approach (Law et al. 1990; Desai 2000; Kokusho 2013, 2017; Lirer

et al. 2020; Mele 2020). However, these alternative procedures are still confined to scientific discussion and are not usually adopted in engineering practice.

On the other hand, the values of b and β in Eq. 2 can be calculated as functions of the corrected CPT tip resistance and of the corrected SPT blow count as follows (Chiaradonna and Flora 2020):

$$b = -1.487 \cdot 10^{-8} \cdot q_{c1Ncs}^3 + 1.291 \cdot 10^{-5} \cdot q_{c1Ncs}^2 - 5.722 \cdot 10^{-4} \cdot q_{c1Ncs} + 0.163 \quad (6a)$$

$$b = -1.000 \cdot 10^{-6} \cdot (N_1)_{60cs}^3 + 2.216 \cdot 10^{-4} \cdot (N_1)_{60cs}^2 + 1.727 \cdot 10^{-3} \cdot (N_1)_{60cs} + 0.1557 \quad (6b)$$

$$\beta = 0.01166 \cdot FC + 0.3536 \cdot \left(q_{c1Ncs} - \Delta q_{c1N}\right)^{0.264} - 0.2805 \quad (7a)$$

$$\beta = 0.01166 \cdot FC + 0.1091 \cdot \left((N_1)_{60cs} - \Delta (N_1)_{60}\right)^{0.5} + 0.5058 \quad (7b)$$

in which FC is the fine content expressed in percentage.

Once FS is estimated performing a liquefaction assessment analysis via Eq. 3, and known b and β, which depends on state conditions of soils (Eqs. 6, 7), the related pore pressure increments can be quantified through Eq. (2).

It should be specified that Eq. (2) has been obtained with the only assumption that the irregular pore pressure build up history related to irregular acceleration time histories can be modeled as proposed by Booker et al. (1976) for the case of constant amplitude cycles, with a simplifying procedure in all similar to the one adopted by Seed and Idriss (1971) to calculate the liquefaction demand CSR (Eq. 5). The details of the procedure are reported in Chiaradonna and Flora (2020). This approach has been already validated using independent laboratory results obtained for different sands and relative densities, offering a simple yet sound tool to estimate r_u for saturated soils. Figure 1 reports some charts in which Eq. (2) is graphically represented for different values of the fine content FC and different values of either q_{c1Ncs} and $(N_1)_{60cs}$, or alternatively for different values of the relative density D_r.

Since one of the most innovative ground improvement technologies available to reduce liquefaction risk is to decrease the degree of saturation of liquefiable soil layers (S_r), there is the need to extend Eq. (2) to the case of $S_r < 1$ (non-saturated soils), in order to be able to estimate the effectiveness of the remediation measure and tackle all the possible risks related to the reduction of effective stresses (defined using Bishop's notation, Bishop and Blight 1963). This paper will therefore propose a novel relationship, extending Eq. (2) to the case of non-saturated soils and showing all the theoretical considerations and experimental results that have been taken into account to this aim. As will be shown, for non-saturated soils this is never a trivial issue, even for $FS \leq 1$. Finally, a validation of the procedure for both saturated and non-saturated soils will be presented, using the results of centrifuge tests (Fioravante et al. 2020) in which irregular acceleration time histories were used.

2 Pore pressure increments in non-saturated soils at liquefaction triggering

The cyclic resistance of sandy soils is extremely sensitive to the reduction of the degree of saturation as demonstrated in several research works (Chaney 1978; Yoshimi et al. 1989; Ishihara et al. 2002; Yegian et al. 2007; Mele et al. 2018; Mele and Flora 2019). It is due to

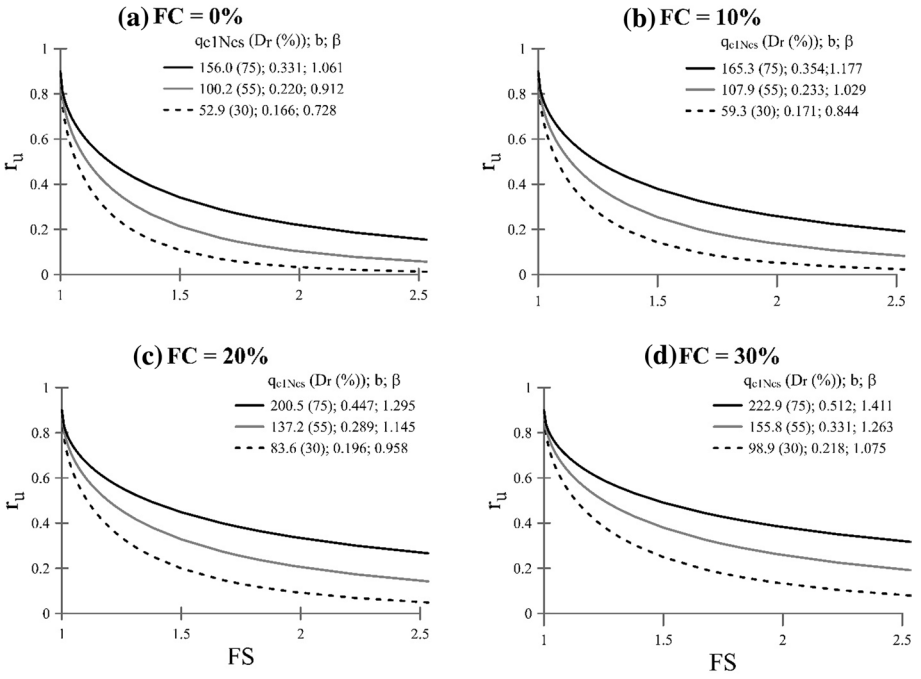

Fig. 1 Charts relating the free field pore pressure ratio r_u and the free field liquefaction safety factor FS for saturated soils ($S_r = 1$) with different fine contents: **a** FC = 0%, **b** FC = 10%, **c** FC = 20%, **d** FC = 30% (mod. after Chiaradonna and Flora 2020)

the presence of air in the voids, which increases the compressibility of fluid phase, reducing the excess pore pressure (Okamura and Soga 2006) and increasing the stiffness and strength of soils (Bishop and Blight 1963) due to a matric suction, defined as the difference between the pore pressure of air and water. The latter mechanism becomes relevant when the degree of saturation is low enough to have a continuous air phase. The soils, in this condition are generally called unsaturated soils (Tsukamoto et al. 2014), to distinguish them from partially saturated soils, characterized to have a continuous water phase. Generally, it happens for Sr higher than 80% (Schuurman 1966; Pietruszczak and Pande 1996; Tsukamoto et al. 2014). With such high values of Sr, the water phase is continuous with dispersed gas bubbles.

Okamura and Soga (2006) suggested to compute the liquefaction resistance of a non-saturated soil CRR_{ns} starting from the one measured for the fully saturated soil CRR as:

$$LRR = \frac{CRR_{ns}}{CRR} = \log(6500 \cdot \varepsilon_v^* + 10) \tag{8}$$

where LRR is defined as the liquefaction resistance ratio, which is the ratio of the liquefaction resistance (defined as the cyclic stress ratio to cause $\varepsilon_{DA} = 5\%$ in 20 cycles) of a non-saturated sand normalized with respect to that of a fully saturated sand, and ε_v^* is the potential volumetric strain. The potential volumetric strain (ε_v^*) represents the highest value of the volumetric strain of the non-saturated soils achieved when the effective stresses are zero.

The potential volumetric strain of the non-saturated sand can be quantified via the Boyle's law as:

$$\varepsilon_v^* = \frac{e_0}{1+e_0} \cdot \left(1 - S_{r0}\right) \cdot \left(1 - \frac{u_{a,0}}{\sigma}\right) \tag{9}$$

where $u_{a,0}$ is the initial air pressure and σ is the total stress.

In this paper, the attention is mainly focused on IPS technique, which consists of introducing bubbles of gas into the voids of the soil, to achieve partially saturated soils (bubbles occluded) in order to increase the resistance to liquefaction. In other words, the target of IPS is usually to decrease the saturation degree (Sr) to values not lower than 80%.

From a mechanical point of view, this means that there is no mechanical effect of suction on soil skeleton, even though air and water pressure are slightly different. This is confirmed by the soil water retention curves shown by Mele et al. (2018), who performed non-saturated cyclic triaxial tests on soils with different gradings (Sant'Agostino sand; bauxite and Inagi sand; see Fig. 2a and Table 1). Focusing the attention on the soil water retention curve of Sant'Agostino sand (Fig. 2b), for instance, it can be noted that suction is very low ($s \approx 3$ kPa) even for S_r as low as 55%, confirming that it can be neglected in the usual applications of IPS.

In undrained cyclic tests on non-saturated loose soils, the soil volume will decrease inducing an increase of the degree of saturation: the definition of liquefaction in this case is less straightforward than for saturated soils. Mele (2020) has shown that the stress based ($r_{u,liq} = 0.9$ to trigger liquefaction) and the strain based approach (double amplitude strain $\varepsilon_{DA} = 5\%$ to trigger liquefaction) lead to the same result as long as the soil is saturated, while the difference between the two approaches increases as S_r decreases. For non-saturated soils, the condition $r_{u,liq} = 0.9$ always corresponds to a higher number of cycles to liquefaction, and to an unrealistically high strain level. Therefore, when testing on non-saturated soils, the strain-based criterion is generally used to define liquefaction triggering (Mele et al. 2018), and therefore it will be assumed that $r_{u\text{-}liq} = r_u(\varepsilon_{DA} = 5\%)$. As a consequence, liquefaction triggering will correspond to values of $r_{u,liq} \leq 0.9$ and therefore to values of the effective stress at liquefaction (Bishop notation) $\sigma'_{liq} \geq 0.1\sigma'_0$, where σ'_0 is the initial effective confining stress. Obviously, because of this pore pressures will continue to increase upon liquefaction attainment.

On the basis of the experimental evidences presented by Mele et al. (2018), obtained by means of cyclic tests on different soils (Sant'Agostino sand; bauxite and Inagi sand; see Fig. 2a and Table 1 and water retention curves in Fig. 2b) reconstituted at different state conditions with an initial degree of saturation S_{r0} higher than 50% ("Appendix 1"), Mele and Flora (2019) proposed a simple way to estimate the effective stress corresponding to liquefaction triggering σ'_{liq} through the following equation:

$$\frac{\sigma'_{liq}}{\sigma'_0} = -2 \cdot 10^{-4} \cdot S_{r0}^2 + 2 \cdot 10^{-2} \cdot S_{r0} + 0.10 \tag{10}$$

Equation (10) does not explicitly take into account the effect of relative density, that should play a role in the pore pressure build up mechanism, because the influence of S_{r0} is so large to shadow it, at least for loose to medium dense sands, for which liquefaction may be a concern (Mele 2020).

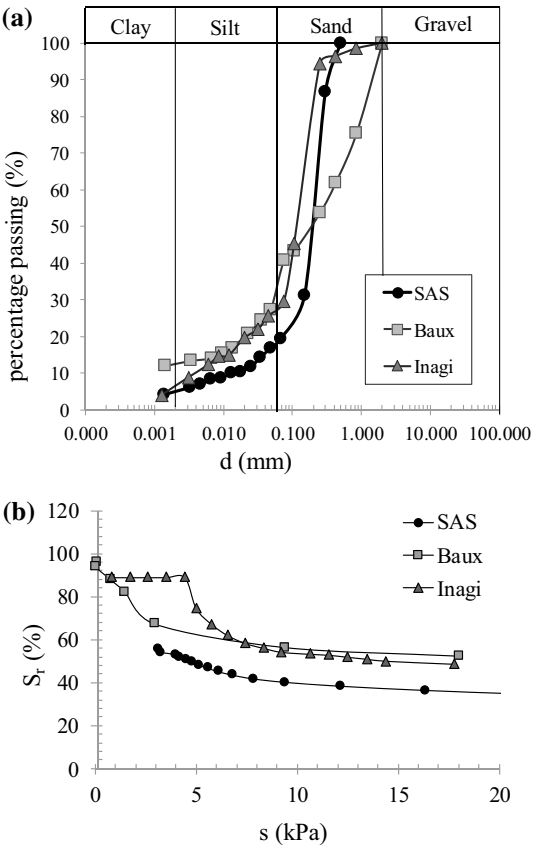

Fig. 2 **a** Grain size distribution curves of Sant'Agostino (SAS), bauxite (Baux) and Inagi sand (Mele et al. 2018). **b** Soil–water retention curve (SWRC) of tested soils (Mele et al. 2018)

Table 1 Material properties of the soils (Mele et al. 2018)

Material property	Sant'Agostino sand	Bauxite	Inagi sand
Fines content FC (< 0.075 mm) (%)	20.0	40.6	29.5
Specific gravity (G_S)	2.674	2.642	2.656
D_{50} (mm)	0.200	0.200	0.115
e_{max}	1.01	–	1.645
e_{min}	0.37	–	0.907

Since this paper is concerned with the pore pressure build up mechanism, recalling that $r_{uliq} = 1 - \sigma'_{liq}/\sigma'_0$ (where $r_{u,liq}$ is the value of r_u at the triggering of liquefaction) Eq. (10) can be rewritten as:

$$r_{u,liq} = 2 \cdot 10^{-4} \cdot S_{r0}^2 - 2 \cdot 10^{-2} \cdot S_{r0} + 0.90 \tag{11}$$

Figure 3 reports a comparison between the experimental results and Eq. (11). The agreement is satisfactory in the whole range of degrees of saturation for which it can be assumed to hold ($55\% < S_{r0} \leq 100\%$), and particularly in the range most interesting for

IPS (i.e.,$80\% \le S_{r0} \le 100\%$), in which there is an almost linear relationship between $r_{u,liq}$ and S_{r0}.

For $S_{r0} = 100\%$ Eq. (11) leads to $r_{u,liq} = 0.9$, consistently with the stress based definition of liquefaction triggering. Equation (11) is a simple tool to estimate pore pressure increments when FS = 1 for loose and medium dense sands having any initial degree of saturation in the range $55\% \le S_{r0} \le 100\%$.

3 Pore pressure increments in non-saturated soils before liquefaction

For saturated soils, cyclically induced pore pressure build-up is usually expressed using the model proposed by Booker et al. (1976) (Eq. 1). For non-saturated soils, the experimental evidences show that from a mathematical point of view, a similar expression should hold, with the main difference that the value of $r_{u\ liq}$ is not a constant but a function of S_{r0} (Eq. 11). Figure 4, for instance, reports the comparison of four undrained cyclic triaxial tests carried out on saturated (Mele et al. 2018; Lirer and Mele 2019; Table 5 in "Appendix 1") and non-saturated specimens of Sant'Agostino sand (Mele et al. 2018, as shown in Table 6, "Appendix 1"). The tests have been selected based on the number of cycles N, in order to have one saturated and one non-saturated test liquefying at a similar (Fig. 4a) or at the same (Fig. 4b) value of N (obviously obtained using different values of CSR) (Tables 5, 6 in "Appendix 1").

As expected, saturated specimens exhibit a more evident increase of the excess pore pressure ratio, and non-saturated specimens reach lower values of $r_{u,liq}$ at liquefaction. In Fig. 5, the same results of Fig. 4 are reported in a normalized plot (N/N_{liq}: $r_u/r_{u,liq}$), where the pore pressure increment ratio r_u and the number of cycles N have been divided by their values at liquefaction.

In these normalized plots, the pore pressure increments of saturated and non-saturated specimens show a similar trend, with the results of the non-saturated tests plotting just a little below those of the saturated ones. Assuming a unique trend for all the tests, the following formal correlation can be written:

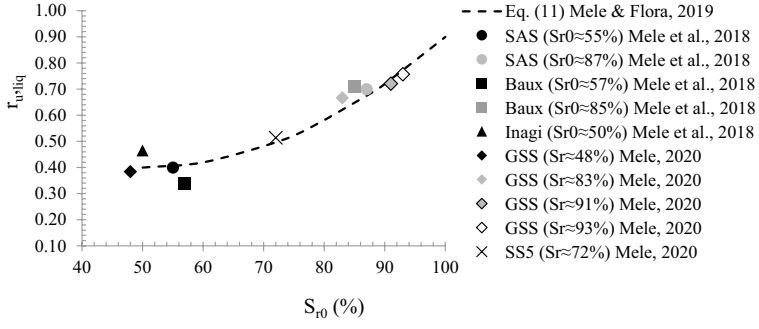

Fig. 3 Experimental values of $r_{u\text{-}liq}$ and S_{r0} published by Mele et al. (2018) and Mele (2020) along with the best fitting curve proposed by Mele and Flora (2019). GSS = grey silty sand coming from Pieve di Cento (Italy); SS5 = silica sand (N0 5), further details can be found in Mele (2020). $r_{u,liq}$ is associated with $\varepsilon_{DA} = 5\%$

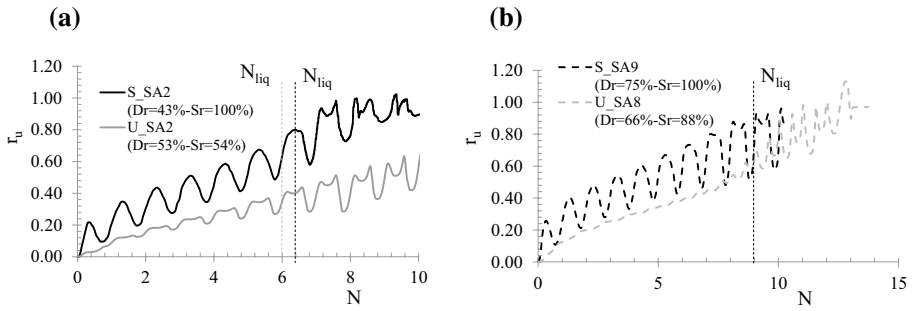

Fig. 4 Comparisons between the excess pore pressure build-up of saturated and non-saturated soils, which attained liquefaction at similar (**a**) or the same (**b**) number of cycles

Fig. 5 Comparisons between the excess pore pressure build-up of saturated and non-saturated soils, in the normalized plane N/N_{liq}:$r_u/r_{u,liq}$

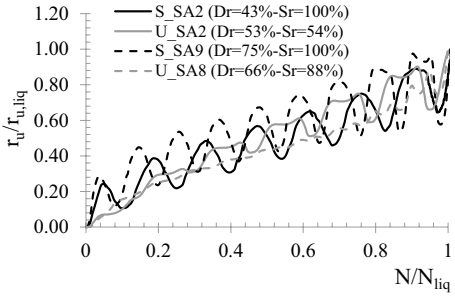

$$\left(\frac{r_u}{r_{u,liq}}\right)_{ns} = \left(\frac{r_u}{r_{u,liq}}\right)_{s} \tag{12}$$

where $r_{u,liq}$ is given by Eq. (11). Equation (12) states that, for a given soil, the parameter β ruling the mathematical expression of pore pressure ratio increment (Booker et al. 1976) does not depend on the degree of saturation as demonstrated by Mele (2020). Therefore, the pore pressure increment of a non-saturated specimen can be computed at any number of cycles $N \le N_{liq}$ as:

$$\begin{aligned} r_{u,ns} &= r_{u,s} \cdot \frac{\left(2 \cdot 10^{-4} \cdot S_{r0}^2 - 2 \cdot 10^{-2} \cdot S_{r0} + 0.90\right)}{0.90} \\ &= \frac{2}{\pi} \cdot \arcsin\left(\frac{N}{N_{liq}}\right)^{\frac{1}{2\beta}} \cdot \left(2 \cdot 10^{-4} \cdot S_{r0}^2 - 2 \cdot 10^{-2} \cdot S_{r0} + 0.90\right) \end{aligned} \tag{13}$$

Figure 6 shows the comparison between Eq. (13) and the results of some tests on non-saturated specimens of Sant'Agostino sand. The prediction of excess pore pressure build-up seems to satisfactorily agree with the experimental data, even though it is worth noting that the simulations cannot go beyond N_{liq} ($\varepsilon_{DA} = 5\%$), because the domain of definition of Eq. (13) is $0 \le N/N_{liq} \le 1$.

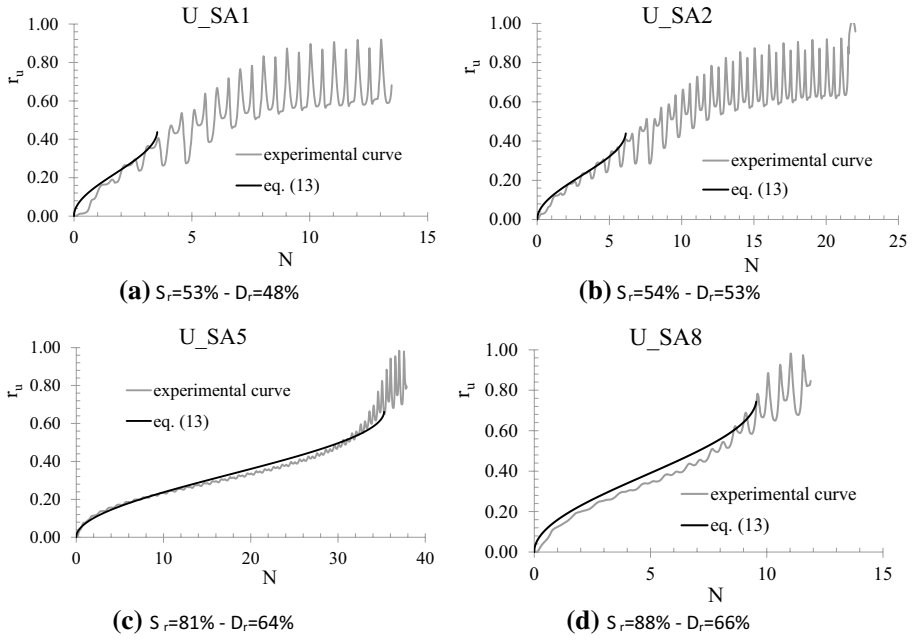

Fig. 6 Comparisons between the experimental and simulated (Eq. 13) excess pore pressure build-up of unsaturated tests on Sant'Agostino sand performed by Mele et al. (2018)

Since r_u is also expressed by Eq. (2) in saturated conditions, the final expression of the pore pressure ratio at any number of cycles and any degree of saturation as a function of the liquefaction safety factor FS is:

$$r_u = \frac{2}{\pi}\arcsin\left(FS^{-\frac{1}{2b_{ns}\beta}}\right)\cdot\left(2\cdot10^{-4}\cdot S_{r0}^2 - 2\cdot10^{-2}\cdot S_{r0} + 0.90\right) \quad \text{with} \quad FS \geq 1 \tag{14}$$

where obviously, FS and b_{ns} are now referred to any degree of saturation ($S_{r0} \leq 100\%$). Then, there is the need to check if b_{ns} assumes the value given by Eq. (6) or depends on S_{r0}.

Mele and Flora (2019) suggest that, as long as a limited range of N is considered (and this is usually the case, being the range $0 \leq N \leq 15$ the most interesting from a practical point of view) the modification of CRR caused by desaturation can be considered as an upwards translation of the cyclic resistance curve CRR(N). This infers a change of the value of b as the degree of saturation changes. Therefore, b_{ns} differs from b and is not constant.

Based on the regression of a large number of experimental data reported by Mele (2020), the following correlation can be assumed:

$$b_{ns} = \left(-3.33\cdot10^{-8}\cdot q_{c1Ncs}^3 + 7.69\cdot10^{-6}\cdot q_{c1Ncs}^2 - 3.07\cdot10^{-4}\cdot q_{c1Ncs} - 0.0376\right)\cdot\exp\left(0.0133\cdot S_{r0}\right) \tag{15}$$

Figure 7 shows charts of r_u-FS for different values of S_{r0}, FC, D_r. The curves have been plotted via Eq. (14), assuming for b_{ns} values given by Eq. (15).The charts have been plotted for the range $20\% \leq D_r \leq 70\%$. Moreover, they are reported in the range of

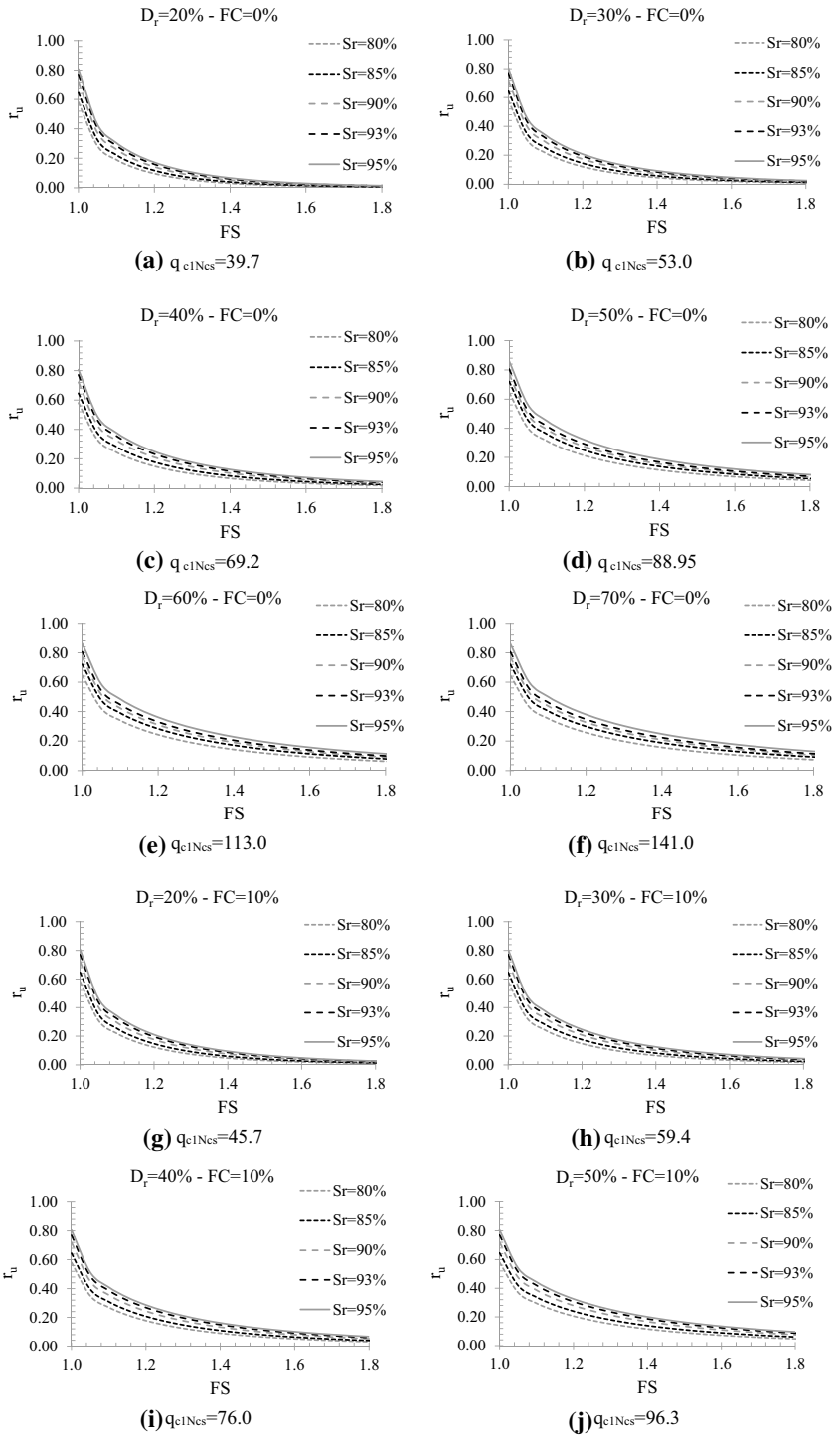

Fig. 7 r_u-FS charts for different values of S_{r0}, FC, D_r

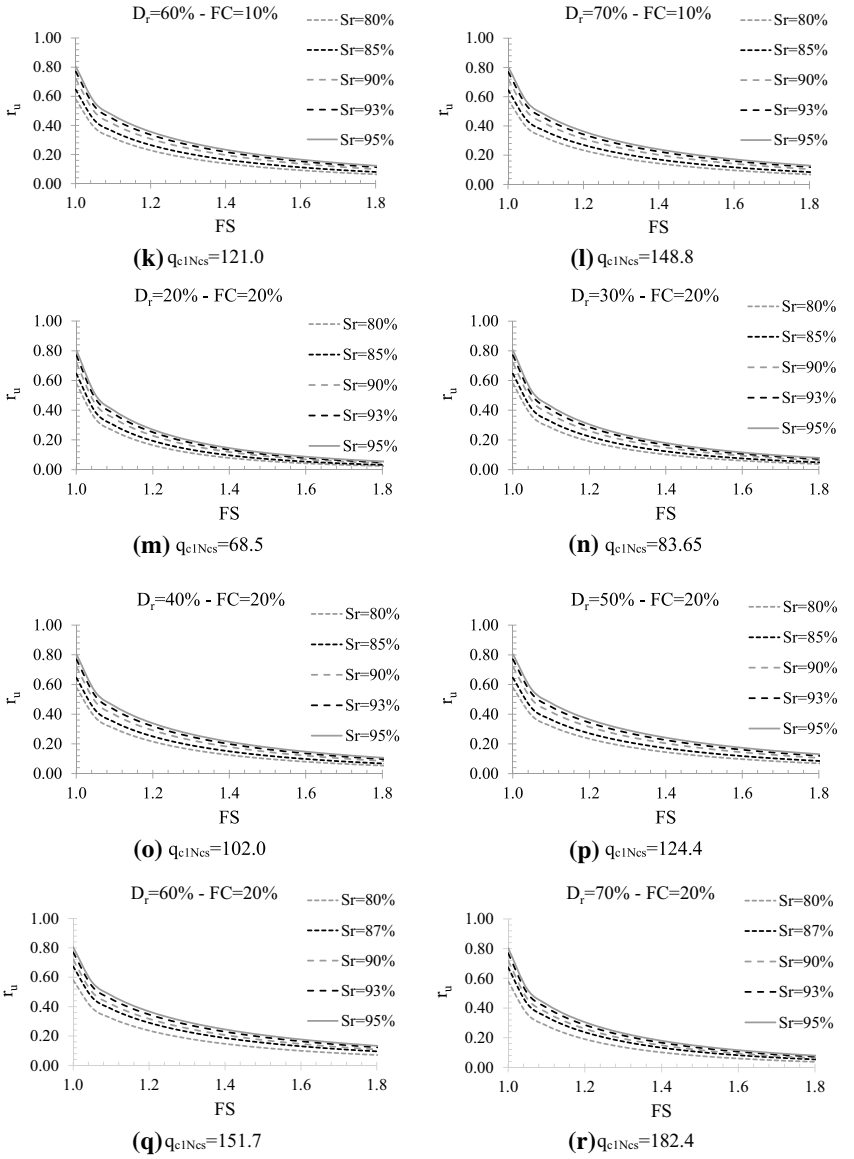

Fig. 7 (continued)

partially saturated soils ($80\% \leq S_r \leq 95\%$), which is of engineering interest in field of IPS.

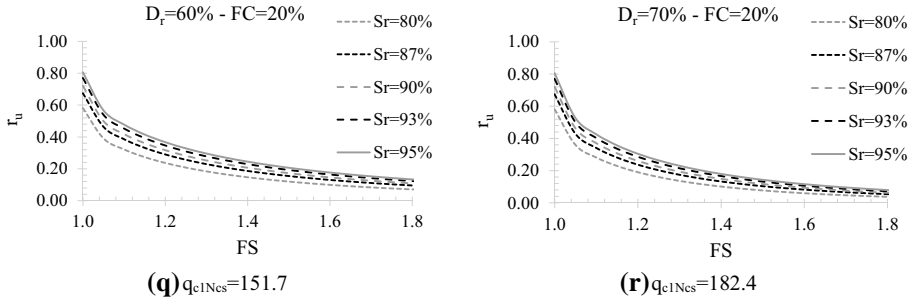

Fig. 7 (continued)

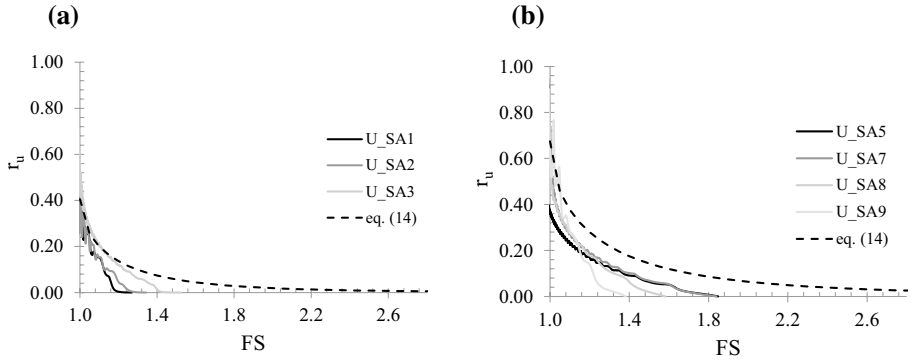

Fig. 8 Comparisons between the experimental and simulated (Eq. 14) curves r_u-FS for Sant'Agostino sand at two different $S_{r,0}$: 55% (unsaturated tests) (**a**) and 87% (partially saturated tests) (**b**)

4 Experimental validation on laboratory tests

Equation (14) has been verified against independent laboratory test results carried out on non-saturated soils. In Fig. 8 the experimental curves obtained at $S_{r0} = 55\%$ (Fig. 8a) and $S_{r0} = 87\%$ (Fig. 8b) on Sant'Agostino sand have been compared with the analytical prediction (Eq. 14), in which b_{ns} has been quantified using Eq. (15). The fitting is quite good for safety factors just higher than 1, becoming less accurate at higher values of FS. In any case, Eq. (14) bounds in a conservative way the experimental results.

As already mentioned above, Eq. (14) does not allow to predict the values of r_u for $FS < 1$. However, this is a minor drawback, because desaturation is adopted as a ground improvement means to modify unsatisfactory site conditions, certainly having the goal to obtain $FS \geq 1$ after the IPS treatment.

5 Experimental validation on centrifuge tests

From a practical point of view, it is of the outmost interest to verify the validity of Eq. (14) against irregular cyclic stress histories, that better resemble real site conditions during seismic shaking. To this aim, two centrifuge tests were used, one carried out on a saturated natural silty sand and the other on a non-saturated clean sand ($Sr \approx 88\%$). The tests were carried out at ISMGEO, in the framework of the European project Liquefact, and are described among others in detail in Fioravante et al. (2020). An Equivalent Shear Beam (ESB) container was used, and the soil models were reconstituted at 1 g to the target relative density ($D_r \approx 56\%$) and then spun up to a centrifuge acceleration of 50 g, as detailed in Fasano et al. (2018) and Fioravante et al. (2020).

Figure 9 shows the test configurations at the prototype scale and the location of the sensors used in the tests (horizontal accelerometers, pore pressure transducers and displacement transducers). Fioravante et al. (2020) also report the details about the procedure applied in the centrifuge test to desaturate the soil (Fig. 9b).

The silica silty sand ($G_S = 2.69$, $U_c = 1.8$, $FC = 12\%$) used for the saturated test was retrieved from a site that experienced liquefaction after the 2012 Emilia earthquake, close to the town of Pieve di Cento, in the Emilia-Romagna region (Italy).

The clean sand ($G_S = 2.65$, $U_c = 1.31$, $FC = 0\%$) used in the non saturated test is the Ticino sand, a uniform coarse to medium sand made of angular to subrounded particles, widely characterized in previous studies (e.g., Fioravante and Giretti 2016).

In order to compare the experimental results with the prediction obtained using Eq. (14), the experimental r_u-FS curves for the two centrifuge tests have to be defined, both for saturated and non-saturated soils. This is not a trivial issue, since the acceleration time histories applied at the base of the container were irregular. The procedure implemented to this aim is reported in the next section, while the comparison with the analytical prediction (Eq. 14) is shown in the subsequent one.

5.1 Calculation of the safety factor for an irregular loading

The determination of the instantaneous safety factor during the application of an irregular loading history is a challenging issue since, by definition (Eq. 3), the safety factor is the ratio between two normalized stress amplitudes (CRR and CSR) which do not depend on time.

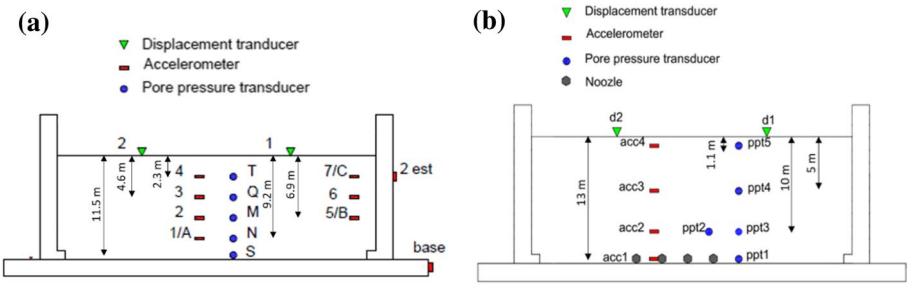

Fig. 9. Cross section of the model configuration in the **a** saturated, **b** non-saturated centrifuge test

The first possibility to overcome this difficulty is to transform the irregular loading into an equivalent number of cycles having an amplitude equal to 65% of its maximum shear stress. The number of cycles could be defined as the one producing an increase of pore pressure equal to that cumulated at the end of the irregular time history. One of the large number of procedures developed for evaluating the equivalent number of cycles (e.g., Seed et al. 1975a; Annaki and Lee 1977; Liu et al. 2001; Green and Terri 2005) could be adopted. Then, to define the safety factor it is also needed to know the CRR(N) curve to finally obtain, with some analytical manipulation, the r_u-FS correlation for saturated ($r_{u,s}$) and unsaturated ($r_{u,ns}$) soils.

The second possibility, here adopted, consists in expressing the safety factor as a function of an accumulation variable depending on time and applicable for any loading pattern. In this case, the accumulation variable proposed by Chiaradonna et al. (2018), i.e., the normalized damage parameter κ/κ_L, will be adopted.

The model formulation implies that, for a harmonic stress history with a constant amplitude *CSR*, a damage parameter κ can be defined, which is proportional to the number of cycles N through the following correlation:

$$\kappa = 4N \cdot \left(CSR - CSR_t\right)^{\alpha} \tag{16}$$

where CSR_t is the asymptotic value of the cyclic resistance curve as the number of cycles tends to infinite, and α is the slope of the curve in a log–log plot (Chiaradonna et al. 2018). This expression of the damage parameter can be easily extended to any irregular shear loading history, as described by Chiaradonna et al. (2018) and reported in "Appendix 1" for the sake of clarity.

Moreover, according to the adopted model based on the damage parameter, the number of cycles at liquefaction, N_{liq}, is univocally related to the cyclic resistance ratio, *CRR*, analytically described by the following equation:

$$\frac{\left(CRR - CSR_t\right)}{\left(CSR_r - CSR_t\right)} = \left(\frac{N_r}{N_{liq}}\right)^{\frac{1}{\alpha}} \tag{17}$$

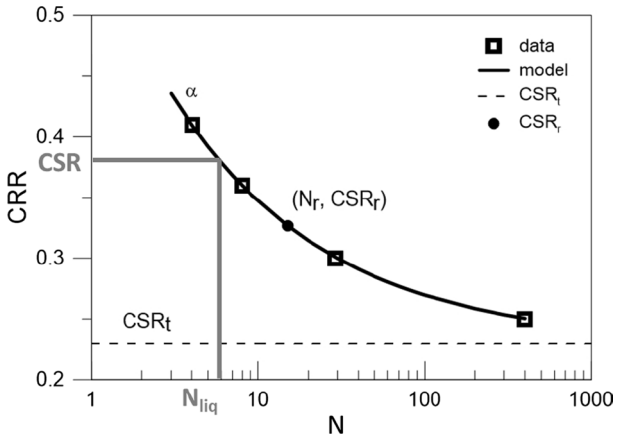

Fig. 10 Cyclic resistance curve and path of a generic uniform loading with amplitude CSR (modified after Chiaradonna et al. 2018)

where (N_r, CSR_r) is a reference point, CSR_t and α the parameters already defined (Fig. 10). In the same figure, a possible value of CSR is reported. For $N = N_{liq}$ (number of cycles at liquefaction) $CRR = CSR$, while for $N < N_{liq}$ $CRR > CSR$.

Combining Eqs. (16) and (17) for $CSR = CRR$, the damage parameter at liquefaction κ_L can be expressed as:

$$\kappa_L = 4N_r \cdot \left(CSR_r - CSR_t\right)^{\alpha} \tag{18}$$

Equation (18) shows that damage at liquefaction assumes a constant value, depending on the parameters describing the cyclic resistance curve (α, CSR_r and CSR_t). Therefore, any point on the cyclic resistance curve is associated to the same damage level κ_L.

In the framework of the damage parameter model, the safety factor can be expressed by manipulating Eq. (17) to express both CRR (for any $N < N_{liq}$) and CSR (= CRR for $N = N_{liq}$) and using it into Eq. (3) as:

$$FS = \frac{CRR}{CSR} = \frac{\left(\frac{N_r}{N}\right)^{\frac{1}{\alpha}}\left(CSR_r - CSR_t\right) + CSR_t}{\left(\frac{N_r}{N_{liq}}\right)^{\frac{1}{\alpha}}\left(CSR_r - CSR_t\right) + CSR_t} \tag{19}$$

Considering Eqs. (16) and (18), the numbers of cycles can be expressed as functions of the damage as follows:

$$N = \frac{\kappa}{\left(CSR - CSR_t\right)^{\alpha}} \tag{20}$$

$$N_{liq} = \frac{\kappa_L}{\left(CSR - CSR_t\right)^{\alpha}} \tag{21}$$

$$N_r = \frac{\kappa_L}{\left(CSR_r - CSR_t\right)^{\alpha}} \tag{22}$$

By substituting the last three relationships in the equation of the safety factor (Eq. 19), it is then obtained that:

$$FS = \left(\frac{\kappa}{\kappa_L}\right)^{-\frac{1}{\alpha}}\left(1 - \frac{CSR_t}{CSR}\right) + \frac{CSR_t}{CSR} \quad \text{with} \quad CSR > CSR_t \tag{23}$$

which is the final relationship adopted in this study to estimate the evolution of the safety factor against liquefaction versus the time.

The application of Eq. (23) requires the definition of the ratio CSR for the irregular loading through Eq. (5), and the computation of the time history of the normalized damage parameter. This latter is a direct application of Eq. (18) and of the damage parameter computation (see "Appendix 2").

Table 2 Parameters of pore pressure model for Pieve di Cento and Ticino sand (Eq. 17), calibrated with the back analysis of the centrifuge tests

Soil	α	CSR_t	CSR_r	N_r
Pieve di Cento sand	2.3	0.152	0.32	15
Ticino sand	3.15	0.06	0.121	25

5.2 Experimental r_u-FS curves and comparison with the proposed charts

Application of Eq. (23) requires the definition of the parameters (α, CSR_r and CSR_t) of the pore water pressure model, as described in Sect. 5.1, for the two considered soils. In this case, the pore water pressure parameters have been calibrated through the back-analysis of the centrifuge tests results (Table 2). Figure 11 shows the comparison between the recorded time histories of the pore pressures and those simulated using the model parameters of Table 3. The full description of the numerical simulations is reported in "Appendix 3".

The time histories of the normalized damage parameter κ/κ_L at the depths of the pore pressure transducers have been extracted from the analysis and used in Eq. 23. It is worth to notice that the obtained time histories of FS do not exceed the time instant where the liquefaction is attained (FS = 1), so as the successive dissipation phase is not considered.

For the centrifuge test on the saturated soil, significant values of $r_{u,s}$ were attained only at the depth of 2.3 m from the surface. Therefore, the procedure was applied only for the transducer placed at this depth.

In order to estimate the Cyclic Stress Ratios, CSR, of the irregular loadings at the depths of pore pressure transducers, the measured accelerograms at the same depths were first integrated to compute the time histories of shear stress, as proposed by Zeghal and Elgamal (1994) and Brennan et al. (2005). Then, the CSR has been calculated as a fraction of the maximum shear stress τ_{max} attained during the time history, with the classical procedure:

$$\mathrm{CSR} = 0.65\frac{\tau_{\max}}{\sigma'_{\mathrm{v}}} \tag{24}$$

where σ'v is the vertical effective stress at a given depth.

Once CSR is known, Eq. 23 allows to quantify the safety factor FS as a function of time. Since the experimental time history of pore pressure ratio is known, the r_u-FS correlation computed from the centrifuge test results can be finally obtained. It should be point out that the r_u-FS curves are related to the time histories until the attainment of the liquefaction condition. Figure 12 reports these experimentally based results along with the corresponding theoretical ones (Eq. 2 with $q_{c1Ncs} = 105$ for the saturated soil, considering $D_{r0} = 57\%$ and fine content FC = 10%, and Eq. 14 for the partially saturated one, imposing $D_{r0} = 57\%$ and $S_{r0} = 88\%$). Even though there is not a perfect agreement, the comparison is certainly satisfactory and the prediction conservative, at least in the range of values of safety factors of highest practical engineering interest ($1 \le FS \le 2$).

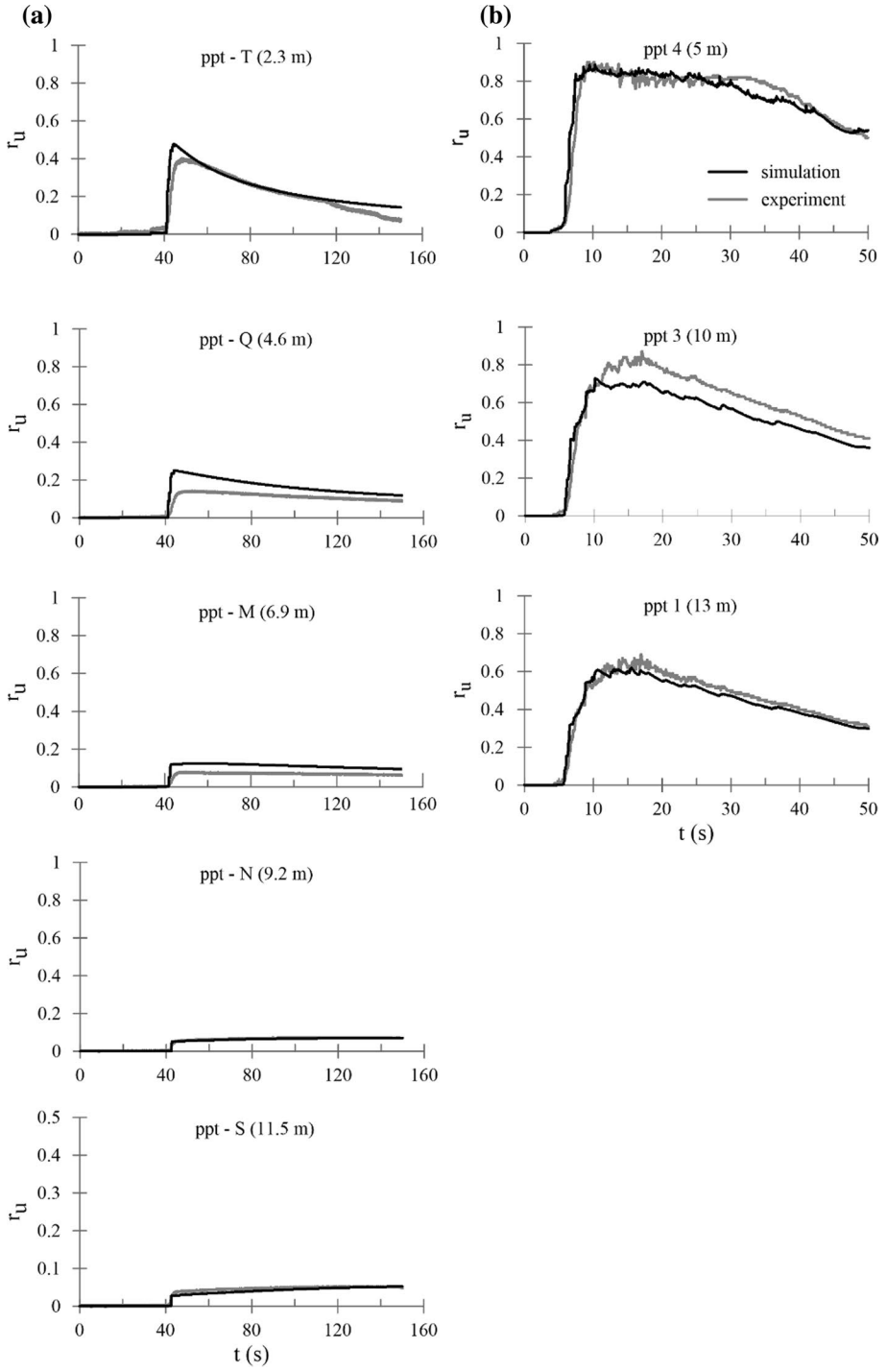

Fig. 11 Recorded and computed excess pore pressure for centrifuge test on **a** saturated, **b** partially saturated sand ($S_r = 88\%$) (measured pore pressure of ppt5 is not accurate and has been neglected)

Table 3 Parameters calculated for Pieve di Cento site (saturated condition) between 2 and 3.5 m from ground surface

z	σ_v*	σ'_v*	q_c	q_{c1Ncs}	$CRR_{M=7.5}$	MSF	K_σ	CRR	r_d	CSR	FS	r_u
m	Figure.	kPa	kPa	–		–	–	–	–	–	–	–
	Figure.				Equation 4a					Equation 5	Equation 3	Equation 2
2.0–2.5	36.9	32.4	962	38	0.08	1.06	1.07	0.10	0.97	0.19	0.49	0.9
2.5–3.0	46.0	36.5	1562	38	0.08	1.06	1.06	0.10	0.97	0.21	0.45	0.9
3.0–3.5	55.2	40.7	3166	54	0.09	1.07	1.07	0.11	0.96	0.23	0.47	0.9

*Total and affective stresses are computed in the middle of the layer

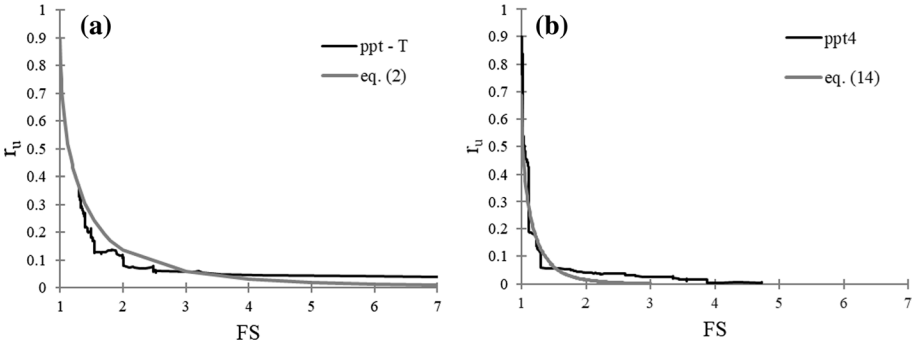

Fig. 12 Comparison between the r_u-FS curves experimentally determined and the proposed analytical correlations for **a** saturated, **b** partially saturated sands

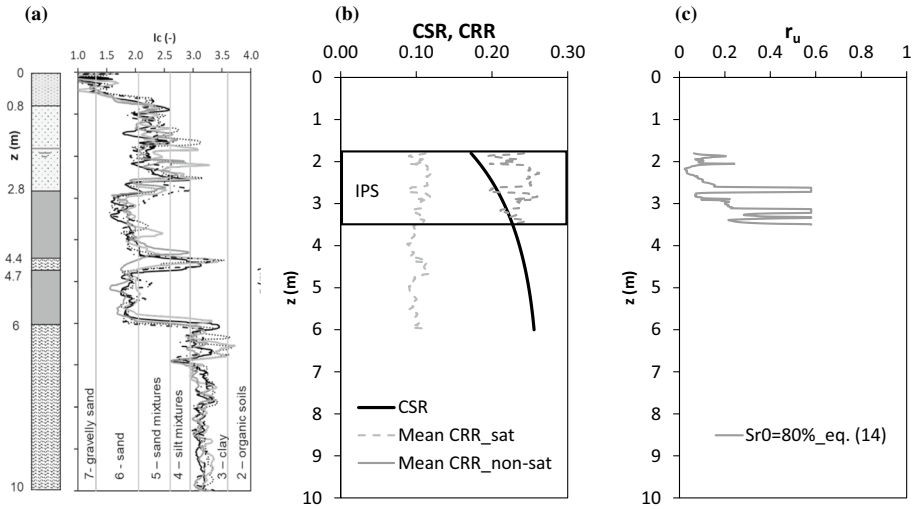

Fig. 13 Pieve di Cento test site: numerical example of field application: Ic (Flora et al. 2020) (**a**), CSR-CRR (**b**) and r_u (**c**) profile

6 Numerical example of field application

Within the European project LIQUEFACT, the effectiveness of induced partial saturation (IPS) in the mitigation of soil liquefaction susceptibility has been verified by means of some large scale shaking tests in a trial field located in Pieve di Cento municipality (Emilia Romagna Region, Italy). An extensive description of the trial field and the performed tests are reported in Flora et al. (2020, this Issue). The representative soil column and the soil behavior index Ic (Robertson 2009) are plotted in Fig. 13a: the critical sandy layer susceptible to liquefaction is located at a depth $1.8 < z < 6.0$ m from the ground surface.

As shown in Flora et al. 2020, the collected CPTU data have been fist used to evaluate liquefaction potential of the Pieve di Cento site for the Emilia 2012 earthquake sequence (occurred on May 20th 2012) using the simplified CPT procedure suggested by Boulanger and Idriss (2014). It can be observed (Fig. 13b) that the results of the liquefaction potential

assessment confirm that the seismic demand CSR of the 2012 Emilia earthquake (Eq. 5) is larger than the soil capacity CRR (Eq. 4a). It should be specified that CSR has been computed for a_{max} equal to 0.27 g, which is the maximum acceleration of the May 20th 2012 earthquake recorded in the surroundings areas of the site (Flora et al. 2020). The values of the main parameters calculated have been summarized in Table 3. The layer between 2 and 3.5 m has been divided in three sublayers. For each of them the average values of the calculated parameters (q_c; q_{c1Ncs}; $CRR_{M=7.5}$; MSF; K_σ; CRR; r_d; CSR) have been reported. As a matter of the fact that FS is lower than 1, r_u is assumed equal to 0.90.

The IPS technique has been applied in the shallow liquefiable sandy layer ($2.0 < z < 3.0$ m) by injection of about 15 m^3 of pressurized air from four horizontal well screens installed by means of the directional drilling technique: this amount of air has been quantified considering the soil volume to be treated and the suited final value of Sr (higher than 80%). By knowing the relative density of the shallow soil layer ($Dr \approx 40\%$, $e_0 = 0.70$) and the expected average value of the degree of saturation ($Sr = 0.8$), the potential volumetric strain ε_v* and the liquefaction resistance ratio LRR have been quantified respectively by means of Eqs. (9) and (8). The liquefaction resistance of the soil volume treated with IPS (CRR_{ns}) has that been obtained starting from the one measured for the fully saturated soil CRR. It can be noted (Fig. 13b) that, as expected, the reduction of the degree of saturation increased the soil capacity that, in the treated soil volume, becomes lower than the 2012 Emilia earthquake demand represented by CSR(z).

The knowledge of the safety factor FS for the treated soil also allows to quantify the expected pore pressure ratio $r_u(z)$ within the layer by means of the Eqs. 6a, 14 and 15. The values of the main parameters have been summarized in Table 4. It should be noted that for $FS = 1$ $r_{u,liq}$ is 0.58.

This example confirms what has been observed in the in situ liquefaction tests (Flora et al. 2020), where the dynamic load has been applied by a shaker machine located at the ground surface. The comparison between the data collected in the large scale shaking tests carried out in the untreated area ($r_{u,max} \approx 0.9$) and in the area treated with IPS ($r_{u,max,IPS} \approx 0.1$) demonstrated that the de-saturation was extremely effective, thus confirming to be a sustainable technique to tackle liquefaction risk in densely urbanized areas.

7 Conclusions

The paper has proposed a simple analytical tool (summarized in the flow chart of Fig. 14) to estimate the pore pressure ratio r_u as a function of the free field safety factor against liquefaction FS for any degree of saturation of the soil and for $FS \geq 1$. As obvious, different equations (respectively Eqs. 2, 14) were obtained for the cases of saturated and non-saturated soils. In the latter case, experimental evidences indicate that liquefaction triggering does not correspond to $r_u = 0.9$, and the values of the pore pressure increments attained at liquefaction depend on the degree of saturation (Eq. 11).

The correlations proposed are simplified in the sense that they have been obtained introducing some simplifying assumptions (one for all: a regular pore pressure build up during the seismic action), but the experimental verification has demonstrated that they are able to capture test results with a reasonable accuracy. To this aim, the results

Table 4 Parameters calculated for Pieve di Cento site (partially-saturated condition) between 2 and 3.5 m from ground surface ($e_0 = 0.700$; $S_{r0} = 80\%$)

z	FC	Δq_{c1N}	u_w	CRR	ε_v*	$LRR_{,20}$	CRR_{ns}	FS	b_{ns}	β	r_u
m	%	–	kPa	–	–	–	–	–	–	–	–
					Equation 9	Equation 8	Equation 8	Equation 3	Equation 15	Equation 7a	Equation 14
2.0–2.5	22.9	27.3	4.5	0.10	0.0217	2.18	0.22	1.16	0.11	0.72	0.07
2.5–3.0	16.8	12.6	9.5	0.10	0.0227	2.20	0.22	1.16	0.11	0.72	0.24
3.0–3.5	0.0	0.0	14.5	0.11	0.0235	2.21	0.24	1.00	0.11	0.72	0.37

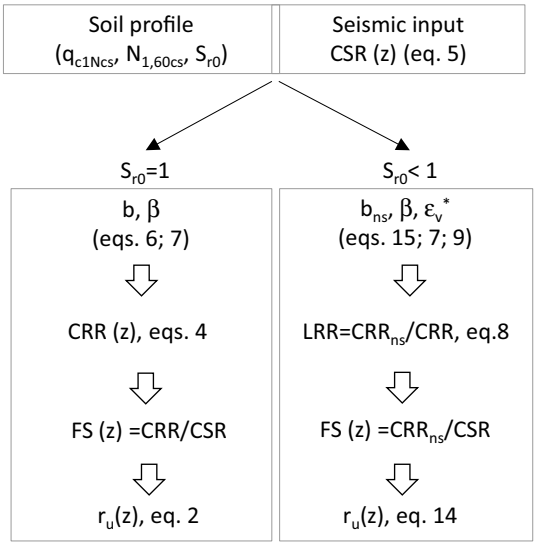

Fig. 14 Proposed flow chart for evaluation of pore pressure ratio r_u in saturated and non saturated soils

Table 5 Results of cyclic saturated tests

Test	σ'_c (kPa)	Dr* (%)	CSR	N_{liq} (ε_{DA} = 5%)	N_{liq} (r_u = 0.9)	References
S_SA1	50	47	0.147	2.7	3	Mele et al. (2018)
S_SA2	51	43	0.128	7.5	7	Mele et al. (2018)
S_SA3	51	46	0.098	19	19	Mele et al. (2018)
S_SA4	51	47	0.087	No	No	Mele et al. (2018)
S_SA5	51	64	0.179	3	3	Mele et al. (2018)
S_SA6	51	59	0.147	13	11.5	Mele et al. (2018)
S_SA7	51	56	0.128	15.5	14	Mele et al. (2018)
S_SA8	50	74	0.198	8	4	Lirer and Mele (2019)
S_SA9	50	75	0.179	–	9	Lirer and Mele (2019)
S_SA10	50	73	0.164	41	28	Lirer and Mele (2019)
S_BA1	49	84**	0.181	6.4	7.6	Mele et al. (2018)
S_BA2	49	85**	0.173	12.3	13.0	Mele et al. (2018)
S_BA3	49	82**	0.163	22.9	23.0	Mele et al. (2018)
S_IN1	59	62	0.160	8.7	9.2	Mele et al. (2018)
S_IN2	58	64	0.142	48.4	50.8	Mele et al. (2018)

*Relative density and degree of saturation after consolidation phase

**Degree of Compaction values (JIS A-1201:1990; JIS: Japan Industrial Standard)

of both laboratory tests carried out applying constant amplitude cycles and centrifuge tests done with irregular acceleration time histories were used.

Equation (2) is of extreme practical interest to estimate pore pressure increments when full liquefaction has not been attained, and therefore to check if the reduction in effective stress may be critical for the site under investigation. In fact, even though the

Table 6 Results of all cyclic non-saturated triaxial tests (Mele et al. 2018)

Test	σ'_{un} (kPa)	D_r* (%)	S_r* (%)	$S_{r,average}$ (%)	CSR	N_{liq} ($\varepsilon_{DA}=5\%$)
U_SA1	49.6	48	53.0	55.0	0.370	3.6
U_SA2	50.5	53	54.0		0.348	6.1
U_SA3	48.9	54	56.0		0.307	26
U_SA4	50.5	63	90.0	87.0	0.160	201
U_SA5	49.8	64	81.5		0.222	35.3
U_SA6	49.8	66	87.2		0.254	11.3
U_SA7	49.9	67	86.7		0.223	24.4
U_SA8	48.8	66	87.6		0.258	9.6
U_SA9	50.4	62	88.5		0.297	2.1
U_BA1	51.9	79**	58.0	56.7	0.353	113.2
U_ BA2	56.3	79**	56.0		0.361	37.3
U_ BA3	51.8	78**	56.0		0.398	12.6
U_ BA4	49.8	88**	84.0	84.5	0.322	0.8
U_ BA5	49.1	85**	85.0		0.279	8.3
U_IN1	62.2	60	49.0	49.7	0.393	13.9
U_ IN2	64.2	58	48.0		0.377	49.6
U_ IN3	62.3	69	52.0		0.404	8.6

*Relative density and degree of saturation after consolidation phase

**Degree of compaction values (JIS A-1201:1990; JIS: Japan Industrial Standard)

procedures discussed in this paper refer to free field conditions, it is possible to estimate a correlation between the free field pore pressure ratio and the one under existing buildings, thus allowing to investigate critical mechanisms (like bearing capacity safety factor reduction, or settlements) that may affect existing structures on liquefiable soils before liquefaction is triggered.

The correlation $r_{u,ns}$-FS for non-saturated soils (Eq. 14) can be considered as a design tool: once in fully saturated conditions, for given values of FS (higher than 1) and D_r, $r_{u,ns}$ is considered to be too high even though liquefaction is not triggered, a target $r_{u,ns}$ (maximum desired value) can be selected and used to choose a target degree of saturation to be reached by induced partial saturation.

Appendix 1: Saturated and non-saturated laboratory tests

In this section, the results of saturated (Mele et al. 2018; Lirer and Mele 2019) and non-saturated (Mele et al. 2018) tests have been summarized in Tables 5 and 6, respectively. Some of such tests have been processed in this paper to extend the charts FS-r_u of Chiaradonna and Flora (2020) for saturated soils to non-saturated ones (Sect. 3). The charts FS-r_u have been also validated on some of such laboratory tests (Sect. 4).

Appendix 2: Calculation of the damage parameter versus time for an irregular shear stress history

For any irregular shear loading history, normalized to the initial effective stress state as:

$$\tau^*(t) = \frac{|\tau(t)|}{\sigma_0'} \tag{25}$$

the damage parameter is calculated as:

$$\kappa(t) = \kappa_0 + d\kappa \tag{26}$$

whereκ_0 is the damage cumulated at the last reversal point of the function $\left(\tau^* - CSR_t\right)$ reached at the time instant t. The parameter κ_0 can be defined as follows:

$$\kappa_0 = \begin{cases} \kappa(t-dt) \text{ if } \dot{\tau}^*(t) = 0 \text{ or } \tau^*(t) = CSR_t \\ \kappa_0(t-dt) \text{ if } \dot{\tau}^*(t) \neq 0 \text{ or } \tau^*(t) \neq CSR_t \end{cases} \tag{26}$$

i.e., κ_0 is a stepwise function assuming the value of the damage parameter gained at the time step (t—dt) every time the stress ratio reaches a local maximum value, or when $\tau^* = CSR_t$ (see Chiaradonna et al. 2018 for details).

The increment of the damage parameter, $d\kappa$, in the time interval dt is given by:

$$d\kappa = \begin{cases} 0 & \text{if } \tau^*(t) < CSR_t \\ \left[\tau_0^*(t) - \tau(t)\right]^\alpha & \text{if } \tau^*(t) \geq CSR_t \end{cases} \tag{27}$$

where $\tau_0^* = \tau_{\max}^*$ if $\tau^{\cdot} * (t) < 0$ and $\tau_0^* = CSR_t$ otherwise.

It is important to point out that the damage parameter reaches the maximum value κ_L (Eq. 18) when liquefaction is attained, and this maximum value cannot be overcome. Consequently, when liquefaction triggers $\kappa/\kappa_L = 1$ and FS = 1.

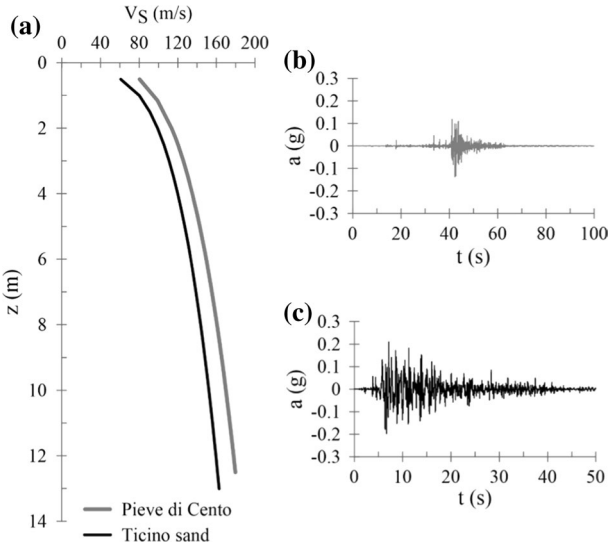

Fig. 15 Profiles of V_S at prototype scale (**a**), acceleration time history of the reference input motion for saturated (**b**) and unsaturated (**c**) centrifuge test

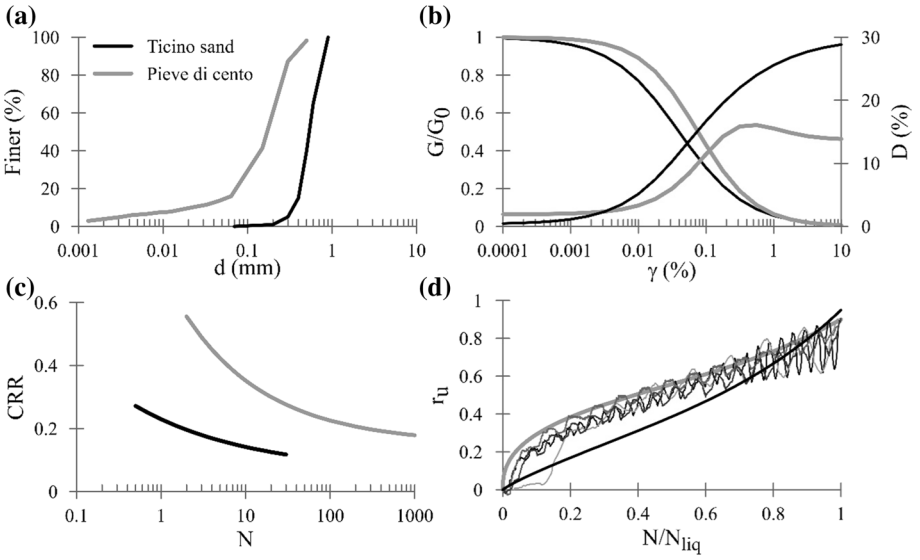

Fig. 16 **a** Grain size distribution, **b** normalized shear modulus and damping ratio vs shear strain, **c** cyclic resistance curve, **d** pore pressure relationships adopted for Pieve di Cento and Ticino sand in the numerical simulations

Appendix 3: Detailed description of centrifuge tests simulations

The centrifuge tests described in Sect. 5 were simulated through a 1D numerical analysis in effective stress conditions using a non-linear computer code in the time domain (Tropeano et al. 2019).

In the simulations, the time history of horizontal acceleration measured at the base of the model (Fig. 15b, c for saturated and unsaturated model, respectively) was applied at the base of the profile (12.5 m and 13 m depth at prototype scale for saturated and unsaturated model), assumed as rigid bedrock. The profile of V_S as a functions of z (Fig. 15a) is characterized by a mean value of approximately 130 m/s, which was calculated as $V_S = L/T$, where L is the distance between the two furthest accelerometers and T is the travel time, as proposed by Ghosh and Madabhushi (2002).

The non-linear and dissipative properties of Pieve di Cento sand (Fig. 16b) were defined based on the experimental data obtained from cyclic laboratory tests, performed on undisturbed samples retrieved on a site 20 km far from Pieve di Cento with the same geological background and a grain size distribution (Chiaradonna et al. 2019). Conversely, the mean curve proposed by Seed and Idriss (1971) for sand has been adopted for Ticino sand, since its grain size distribution is without fine (Fig. 16a).The pore pressure relationship of the model proposed by Chiaradonna et al. (2018) was based on results of cyclic simple shear and cyclic triaxial tests carried out on reconstituted specimens of Pieve di Cento and Ticino sand with a relative density of about 40% (Mele et al. 2019). The pore pressure relationship was calibrated on the experimental data (Fig. 16d) assuming that the influence of relative density on the shape of this curve can be neglected. Finally, a permeability coefficient equal to 1×10^{-5} m/s was estimated and used for Pieve di Cento sand, and 1×10^{-4} m/s for Ticino sand. Once all the input data were known, the cyclic resistance curve adopted for both sands in the analysis has been modified, starting from the available laboratory data,

until the best fitting of the experimental data has been obtained, as discussed in Sect. 5.2. The obtained curves are plotted in Fig. 16c.

References

Annaki M, Lee KL (1977) Equivalent uniform cycle concept for soil dynamics. J Geotech Eng Div ASCE 103(GT6):549–564

Baziar MH, Shahnazari H, Sharafi H (2011) A laboratory study on the pore pressure generation model for Firouzkooh silty sands using hollow torsional test. Int J Civ Eng 9(2):126–134

Bishop AW, Blight GE (1963) Some aspects of effective stress in saturated and partly saturated soils. Gèotechnique 13(3):177–197

Booker JR, Rahman MS, Seed HB (1976) GADFLEA—a computer program for the analysis of pore pressure generation and dissipation during cyclic or earthquake loading. Earthquake Engineering Center, University of California, Berkeley

Boulanger RW, Idriss IM (2014) CPT and SPT liquefaction triggering procedures. Report no UCD/GCM-14/01. University of California at Davis, California

Brennan AJ, Thusyanthan NI, Madabhushi SPG (2005) Evaluation of shear modulus and damping in dynamic centrifuge tests. J Geotech Geoenviron Eng. https://doi.org/10.1061/(ASCE)0733-9410(1994)120:6(996)

Cetin KO, Bilge HT (2012) Cyclic large strain and induced pore pressure models for saturated clean sands. J Geotech Geoenviron Eng 138(3):309–323

Chameau JL, Clough GW (1983) Probabilistic pore pressure analysis for seismic loading. J Geotech Eng 109(4):507–524

Chaney R (1978) Saturation effects on the cyclic strength of sands. In: Proceedings ASCE special conference on earthquake engineering and soil dynamics, New York, pp 342–358

Chiaradonna A, Flora A (2020) On the estimate of seismically-induced pore water pressure increments before liquefaction. Geotech Lett. https://doi.org/10.1680/jgele.19.00032

Chiaradonna A, Tropeano G, d'Onofrio A, Silvestri F (2018) Development of a simplified model for pore water pressure build-up induced by cyclic loading. Bull Earthq Eng. https://doi.org/10.1007/s10518-018-0354-4

Chiaradonna A, Tropeano G, d'Onofrio A, Silvestri F (2019) Interpreting the deformation phenomena of alevee damaged during the 2012 Emilia Earthquake. Soil Dyn Earthq Eng. https://doi.org/10.1016/j.soildyn.2018.04.039

Cubrinovski M, Rhodes A, Ntritsos N, van Ballegooy S (2018) System response of liquefiable deposits. Soil Dyn Earthq Eng. https://doi.org/10.1016/j.soildyn.2018.05.013

De Alba P, Chan CK, Seed HB (1975) Determination of soil liquefaction characteristics by large-scale laboratory tests. Rep. no EERC 75-14, Earthquake Engineering Research Center, Univ. of California, Berkeley, California

Davis RO, Berrill JB (1982) Energy dissipation and seismic liquefaction of sands. Earthq Eng Struct Dyn 1982(10):59–68

Desai CS (2000) Evaluation of liquefaction using disturbed state and energy approaches. J Geotech Geoenviron Eng 126(7):618–631

Dobry R, Pierce WG, Dyvik R, Thomas GE, Ladd RS (1985) Pore pressure model for cyclic straining of sand. Civil Engineering Department, Rensselaer Polytechnic Institute, Troy

Fasano G, Bilotta E, Flora A, Fioravante V, Giretti D, Lai CG, Ozcebe AG (2018) Dynamic centrifuge testing to assess liquefaction potential. In: McNamara et al (eds) Physical modelling in geotechnics. Taylor & Francis Group, London, ISBN 978-1-138-34422-8

Fioravante V, Giretti D (2016) Unidirectional cyclic resistance of Ticino and Toyoura sands from centrifuge cone penetration tests. Acta Geotech 11:953–968. https://doi.org/10.1007/s11440-015-0419-3

Fioravante et al (2020) Submitted in this special issue

Flora A, Bilotta E, Chiaradonna A, Lirer S, Mele L, Pingue L (2020) A Field trial to test the efficiency of induced partial saturation and horizontal drans to mitigate the susceptibility of soils to liquefaction. Bull Earthq Eng. https://doi.org/10.1007/s10518-020-00914-z

Ghosh B, Madabhushi SPG (2002) An efficient tool for measuring shear wave velocity in the centrifuge. In: Phillips R, Guo PJ, Popescu R (eds) Proc Int Conf on Phys Modelling in Geotechnics. Balkema, Rotterdam, pp 119–124

Green RA, Terri GA (2005) Number of equivalent cycles concept for liquefaction evaluations-revisited. J Geotech Geoenviron Eng ASCE 131(4):477–488

Green RA, Mitchell JK, Polito CP (2000) An energy-based pore pressure generation model for cohesionless soils. In: John Booker memorial symposium developments in theoretical geomechanics, Rotterdam, pp 383–390

Idriss IM, Boulanger RW (2008) Soil liquefaction during earthquakes. Monograph, Earthquake Engineering Research Institute (EERI), Oakland

Ishihara K, Tsukamoto Y, Nakazawa H, Kamada K, Huang Y (2002) Resistance of partly saturated sand to liquefaction with reference to longitudinal and shear wave velocities. Soils Found 42(6):93–105

Kokusho T (2013) Liquefaction potential evaluations: energy-based method versus stress-based method. Can Geotech J 50(10):1088–1099

Kokusho T (2017) Liquefaction potential evaluations by energy-based method and stress-based method for various ground motions: supplement. Soil Dyn Earthq Eng 95:40–47

Law KT, Cao YL, He GN (1990) An energy approach for assessing seismic liquefaction potential. Can Geotech J 27(3):320–329

Lee KL, Albaisa A (1974) Earthquake induced settlements in saturated sands. J Geotech Geoenviron Eng 100:10496

Liyanapathirana DS, Poulos HG (2002) A numerical model for dynamic soil liquefaction analysis. Soil Dyn Earthq Eng 22(9–12):1007–1015

Lirer S, Mele L (2019) On the apparent viscosity of granular soils during liquefaction tests. Bull Earthq Eng. https://doi.org/10.1007/s10518-019-00706-0

Lirer S, Chiaradonna A, Mele L (2020) Soil liquefaction: from mechanisms to effects on the built environment. Italian Geotech J. https://doi.org/10.19199/2020.2.0557-1405.025

Liu AH, Stewart JP, Abrahamson NA, Moriwaki Y (2001) Equivalent number of uniform stress cycles for soil liquefaction analysis. J Geotech Geoenviron Eng ASCE 127:1017–1026

Martin GR, Finn WL, Seed HB (1975) Fundementals of liquefaction under cyclic loading. J Geotech Geoenviron Eng 101:11231

Mele L (2020) Experimental and theoretical investigation on cyclic liquefaction mechanisms and on the effects of some mitigation measures. PhD thesis, University of Napoli, Federico II, Napoli

Mele L, Flora A (2019) On the prediction of liquefaction resistance of unsaturated sands. Soil Dyn Earthq Eng. https://doi.org/10.1016/j.soildyn.2019.05.028

Mele L, Tan Tian J, Lirer S, Flora A, Koseki J (2018) Liquefaction resistance of unsaturated sands: experimental evidence and theoretical interpretation. Géotechnique. https://doi.org/10.1680/jgeot.18.p.042

Mele L, Lirer S, Flora A (2019) The effect of confinement in liquefaction tests carried out in a cyclic simple shear apparatus. Proceedings of the 7th international symposium on deformation characteristics of geomaterials, Glasgow

NASEM (National Academies of Sciences, Engineering, and Medicine) (2016) State of the art and practice in the assessment of earthquake-induced soil liquefaction and its consequences. National Academies of Sciences, Engineering, and Medicine, Washington, DC. https://doi.org/10.17226/23474

Okamura M, Soga Y (2006) Effects of pore fluid compressibility on liquefaction resistance of partially saturated sand. Soils Found 46(5):695–700

Pietruszczak S, Pande GN (1996) Constitutive relations for partially saturated soils containing gas inclusions. J Geotech Eng 122(1):50–59

Polito CP, Green RA, Lee J (2008) Pore pressure generation models for sands and silty soils subjected to cyclic loading. J Geotech Geoenviron Eng 134(10):1490–1500

Robertson PK (2009) Interpretation of cone penetration tests—a unified approach. Can Geotech J 46(11):1337–1355

Robertson PK, Wride CE (1998) Evaluating cyclic liquefaction potential using the cone penetration test. Can Geotech J 35(5):442–459

Schuurman IE (1966) The compressibility of an air/water mixture and a theoretical relation between the air and water pressures. Geotechnique 16(4):269–281

Seed HB, Idriss IM (1971) Soil moduli and damping factors for dynamic response analysis. Report no EERC 70-10, University of California, Berkeley

Seed HB, Idriss IM, Makdisi F, Banerjee N (1975a) Representation of irregular stress time histories by equivalent unifrom stress series in liquefaction analyses. Earthquake Engineering Research Center, University of California, Berkeley

Seed HB, Martin PP, Lysmer J (1975b) The generation and dissipation of pore water pressures during soil liquefaction. Rep. no. EERC 75-26, Univ. of California, Berkeley

Tropeano G, Chiaradonna A, d'Onofrio A, Silvestri F (2019) Numerical model for non-linear coupled analysis on seismic response of liquefiable soils. Comput Geotech 105:211–227. https://doi.org/10.1016/j.compgeo.2018.09.008

Tsukamoto Y, Kawabe S, Matsumoto J, Hagiwara S (2014) Cyclic resistance of two unsaturated silty sands against soil liquefaction. Soils Found 54(6):1094–1103

Wang JN, Kavazanjian E Jr (1989) Pore pressure development during non-uniform cyclic loading. Soils Found 29(2):1–14

Yegian MK, Eseller-Bayat E, Alshawabkeh A, Ali S (2007) Induced-partial saturation for liquefaction mitigation: experimental investigation. J Geotech Geoenviron Eng ASCE 133(4):372–380

Yoshimi Y, Yanaka K, Tokimatsu K (1989) Liquefaction resistance of partially saturated sand. Soils Found 29(2):157–162

Youd TL (1972) Compaction of sands by repeated shear straining. J Soil Mech Found Div 98(SM7):709–725

Zeghal M, Elgamal A (1994) Analysis of site liquefaction using earthquake records. J Geotech Eng 120:996–1017

Affiliations

Lucia Mele[1] · Anna Chiaradonna[2] · Stefania Lirer[3] · Alessandro Flora[1]

Anna Chiaradonna
anna.chiaradonna1@univaq.it

Stefania Lirer
s.lirer@unimarconi.it

Alessandro Flora
flora@unina.it

[1] University of Napoli Federico II, Naples, Italy

[2] University of L'Aquila, L'Aquila, Italy

[3] University Guglielmo Marconi, Rome, Italy